Synergistic Photocatalytic Reduction of Hexavalent Chromium Using Graphene Quantum Dots and Formic Acid: Optimization and Kinetics

Silmina Silmina[1], Xi-lin Wu[1], Christine Rolle[1], Feng Chen[1], Hao Wang[1], Silva Khairunnisa[1]

Husni Husin[2], Faisal Abnisa[3]

[1] *College of Geography and Environmental Science, Zhejiang Normal University, Jinhua, 321004, China*

[2]*Department of Chemical Engineering, Universitas Syiah Kuala, Banda Aceh, 23111, Indonesia*

[3] *Department of Chemical and Materials Engineering, Faculty of Engineering, King Abdulaziz University, Rabigh, 21911, Saudi Arabia*

Abstract

Graphene Quantum Dots (GQDs) has garnered a significant deal of interest in environmental remediation, particularly for reducing hexavalent chromium [Cr (VI)] to trivalent chromium [Cr (III)]. This study focused on the photocatalytic process of Cr (VI) degradation using GQDs and Formic Acid (FA) under Uv-vis light. Batch experiments were conducted to observe the photocatalytic process of Cr (VI) degradation under Uv-vis light irradiation at varying concentrations of GQDs, FA, and Cr (VI) and different pH levels. The characterization of GQDs includes PL, XPS, XRD, and Raman Spectroscopy. This research revealed that combining GQDs and FA for the photocatalytic process of Cr (VI) reduction is possible. As expected, this system is more effective with lower concentrations of Cr (VI). When FA was introduced, the Cr (VI) degradation efficiency ratio increased. The GQDs/FA/Uv-vis system gave the highest degradation rate at 91.1% within 30 minutes. It was also observed that the optimum pH of the solution was 5.42, where the GQDs were quickly dissoluble. The photocatalytic reduction matched first-order reaction kinetics with a rate constant (k) of 0.1085 min^{-1} and R^2 of 0.985. The primary radical in the degradation of Cr (VI) in the GQDs/FA/Uv-vis system was $CO_2^{\bullet-}$. These findings highlight the potential of GQDs and FA as efficient catalysts for the photocatalytic reduction of Cr (VI) under Uv-vis light.

Keywords: *Graphene Quantum Dots, Hexavalent Chromium, Formic Acid, Photocatalysis.*

1. Introduction

The presence of high concentrations of chromium (Cr) in wastewater poses significant environmental risks. Cr is commonly found in various industries such as metal coatings, leather tanning, wood preservation, stainless steel production, and manufacturing [1]. In nature, Cr occurs in various oxidation states, varying from -2 to +6; the most common and reliable states are trivalent (III) and hexavalent (VI) of Cr. Among its oxidation states, hexavalent chromium (Cr (VI)) is particularly hazardous to living organisms and can cause environmental damage when released into water and soil [2, 3]. Due to its high toxicity compared to trivalent chromium (Cr (III)), it is crucial to convert Cr (VI) to Cr (III) before disposal [4].

The photocatalytic reduction has emerged as an effective method for wastewater treatment, offering cost-effectiveness and environmental friendliness by avoiding the generation of secondary pollutants. Photocatalysts play a critical role in this process, and materials like Photocatalysis plays a key role in this process, and materials such as titanium dioxide (TiO_2) and zinc oxide (ZnO) have been widely considered for natural wastewater purification [5]. However, these materials are considered scarce resources and face the risk of depletion,

Corresponding author: Silmina Silmina *(minasilmina@gmail.com)*
Received: *3 January 2023*; Revised: *17 July 2023*; Accepted: *21 July 2023*; Published: *22 July 2023*

necessitating the exploration of alternative materials with comparable effectiveness [6]. Therefore, exploring an alternative material that may substitute the effectiveness of TiO_2 and ZnO is essential.

Research into carbon-based zero-dimensional (0D) nanomaterials, such as graphene quantum dots (GQDs), have gained significant attention due to their easy synthesis, large surface area, excellent solubility, and high photostability [7, 8]. GQDs can serve as effective photocatalysts under UV light irradiation and have shown promise in the degradation of Cr (VI) [9, 10]. However, the photocatalytic reduction of Cr (VI) using GQDs alone is limited by the slow kinetic process resulting from the reaction of photo-generated electrons with oxygen [11]. The introduction of a reducing agent is required to solve this limitation. Formic acid (FA) exhibits excellent reducing properties and can promptly reduce Cr(VI) [12]. When FA reacts with photogenerated holes in the photocatalytic process, a carbon dioxide anion radical ($CO_2^{\bullet-}$) is generated, accelerating the reaction rate process and determining the main activity of Cr(VI) reduction [10]. Previous studies have investigated the photocatalytic oxidation of organic dye contaminants using GQDs and the photocatalytic reduction of Cr(VI) using nano-sized TiO_2 and FA [10, 11, 13-15]. However, there are no reveal on the photocatalytic process of Cr(VI) reduction using GQDs in the presence of FA as a reducing agent.

This work aims to characterize GQDs using various characterization techniques such as XPS, XRD, Raman spectroscopy and PL. Furthermore, it attempts to investigate the effects of light irradiation, GQDs concentration, FA concentration, initial Cr(VI) concentration and solution pH on the photocatalytic reduction of Cr(VI). Furthermore, the mechanisms and kinetic rates of the photocatalytic process in Cr (VI) degradation will be explored.

2. Material and Methods

2.1. Chemical and Reagent

The chemicals and reagents used in this research are all analytical grades. GQDs with a 1 mg/mL concentration were sourced from Nanjing XFNANO Materials Tech Co., Ltd. (China). Sodium hydroxide (NaOH), hydrochloric acid (HCl), and formic acid (HCOOH) 88% were sourced from Sinopharm Chemical Reagent Co., Ltd. Furthermore, Shanghai Aladdin Chemical Reagent Company (Shanghai, China) provided potassium dichromate ($K_2Cr_2O_7$) and N-N dimethylaniline (N-N DA).

2.2. Photocatalytic Reduction of Cr (VI)

To prepare the simulated wastewater, a solution of $K_2Cr_2O_7$ was utilized. Different concentrations of $K_2Cr_2O_7$ (80 mg/L, 40 mg/L, and 20 mg/L) were prepared in 50 mL glass beakers. Then, 1 mL of GQDs (1 mg/mL) was added to the solution (GQDs: 1 mL, 2 mL). The mixture was stirred for 20 minutes to achieve adsorption equilibrium. To achieve the desired pH values of 3, 4, and 5.42, the initial pH of the solution was modified by adding either 0.1 M HCl or NaOH.

Before exposing the solution to a Uv-vis light source at $\lambda > 420$ nm, 1 mL of solution was sampled as the initial Cr (VI) concentration at 0 minutes. Subsequently, 1 mL samples were taken at specific intervals of 3 minutes for 30 minutes to analyze the concentration of Cr (VI).

To investigate the effect of adding a reduction agent, 1 mL of 88% formic acid (FA) was added to the solution (FA: 1 mL, 2 mL, and 3 mL), followed by exposure to Uv-vis light.

The absorbance at 350 nm of each Cr (VI) sample was measured using a Uv-vis spectrophotometer. A calibration curve was generated by plotting the absorbance values against the initial Cr (VI) concentrations (Figure 1).

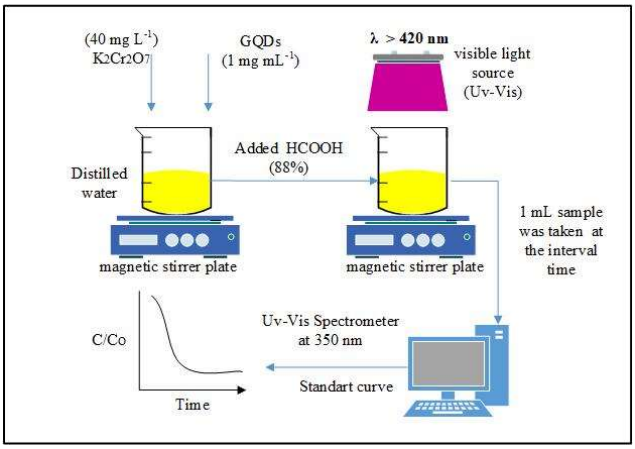

Figure 1. Scheme of Cr (VI) photocatalytic reduction in a batch experiment.

The degradation curve was then obtained using the calibration curve. The photocatalytic reduction efficiency was expressed as C/Co, where Co represents the initial Cr (VI) concentration, and C represents the Cr (VI) concentration at each specific sampling time.

2.3. Instruments and Analytical Methods

X-ray diffraction (XRD) analysis was performed using a Shimadzu XRD X-ray diffractometer, utilizing Cu Kα = 1.54178 radiation to capture a broader range of diffraction peaks for GQDs. Raman spectroscopy was conducted using a Renishaw RM1000 instrument from Renishaw, Hong Kong Co., Ltd, to characterize the carbon nanomaterial properties of GQDs.

X-ray photoelectron spectroscopy (XPS) was carried out using a Thermo Scientific ESCALAB 250 instrument, with Al Kα radiation as the X-ray source, to analyze the elemental composition of GQDs, particularly carbon and oxygen. Photoluminescence (PL) spectroscopy was employed to study the luminescent properties of GQDs, utilizing a SHIMADZU RF-5301PC fluorescence spectrometer. The concentration of Cr (VI) was estimated by measuring its absorbance at 350 nm using a UV-vis spectrometer.

3. Results and Discussion

3.1. Characterization of GQDs

3.1.1. XPS Analysis of GQDs

X-ray photoelectron spectroscopy (XPS) characterized GQDs composition, XPS scans to indicate the presence of the element on the GQDs sample surface [16]. GQDs include three main components, according to several researchers [17] as shown in Figure 2 (a); they are C, N, and O without contaminants at 75.56 %, 0.64%, and 23.8 %, respectively. The high percentage of element C contributes to photocatalytic activity where carbon-based graphene sheets in GQDs can act as excellent conductive pathways for electron/photon transfer [18]. In the XPS full scans spectra, three peaks were detected at 283.40 eV (C1s), 399.10 eV (N1s), and 531.67 eV (O1s).

Figure 2 (b, c) shows the C1s and O1s XPS analysis of GQDs.

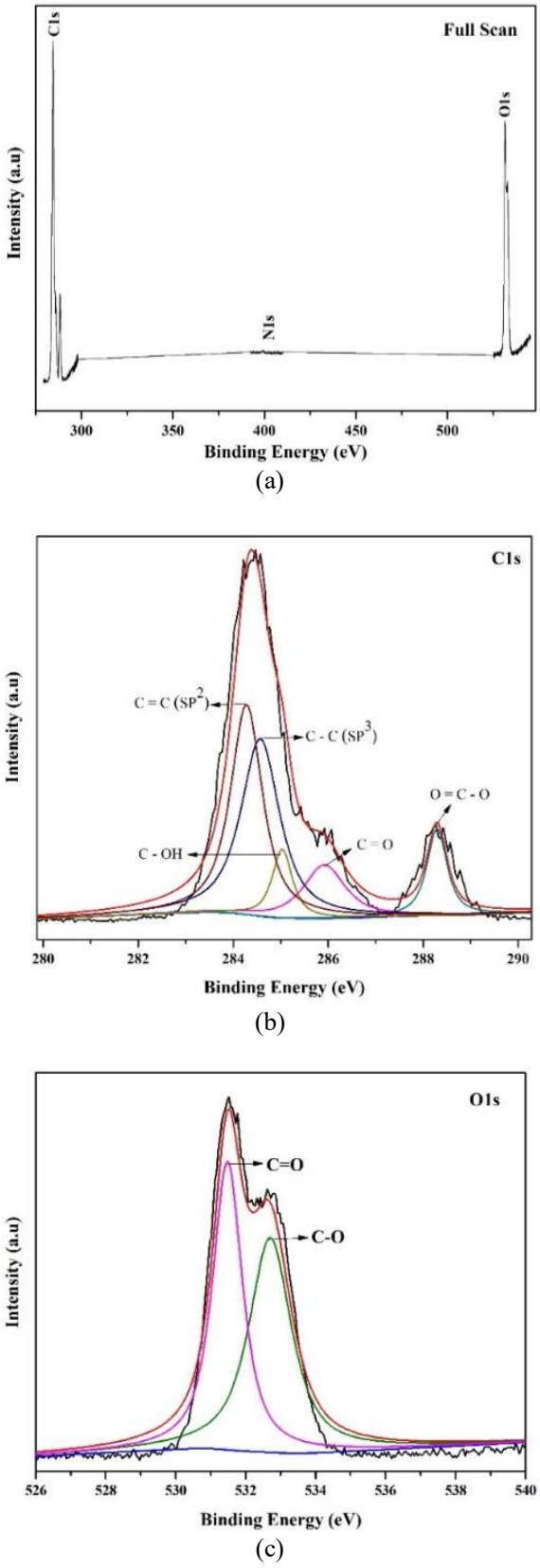

Figure 2. *Full Scan XPS Spectra (a); XPS High-Resolution Deconvolution C1s Spectra (b); and O1s Spectra(c) of GQDs.*

The high-resolution C1s XPS can be separated into five characteristic peaks, such as the signals of sp^2–bonded carbon in C=C (283.28 eV), sp^3–bonded carbon in C-C (283.57 eV), C-OH (285.03 eV), C=O (285.92 eV), and O=C-O (288.52 eV). Meanwhile, the high resolution of the N1s spectrum only shows one peak assigned to pyridinic N (C-N-C) at ~399.1 eV. All sp^2 and sp^3 bonded carbon peaks confirmed graphene hexagonal structure and the aromatic ring group of GQDs, consistent with previous research [19]. The existence of sp^2 and sp^3 C peak in the XPS spectra indicates that GQDs structural planarity has been drastically diminished, and defects have occurred in surface GQDs, which plays the leading role in photocatalytic activity [19, 20]. The high-resolution of the O1s spectrum detects two different peaks at ca. ~531.5 and ~532.7 eV; these peaks are attributed to the presence of C=O bonds and C-OH or C-O [21, 22]. The O1s spectrum results indicate that the GQDs fabricated are common in the oxygen-containing substituents [19].

3.1.2 Raman Spectroscopy Analysis of GQDs

Raman spectroscopy is a crucial characterization to assess GQDs quality. The D and G bands are commonly seen in Raman spectra, and they provide crucial information on the needed quantum point's distinctive form. Figure 3 shows the Raman spectrum of GQDs in the spectral range of 500-2500 cm^{-1}.

The D and G bands, corresponding to sp^2 carbon networks and the graphite structure, were obtained at specific mid-peak points at ca. 1375 and 1589 cm^{-1}, demonstrating its defects and discordance [23, 24]. The intensity ratio of the D and G bands, or I_D/I_G, reveals sp^2 or sp^3 carbon atoms hybridization. The I_D/I_G indicates the crystalline size [25] and estimates GQDs defect rates [26]. The I_D/I_G ratio was obtained at 0.92, expressing a partially disordered graphite structure of GQDs. According to the D and G bands, the Raman spectrum of the GQDs sample exhibits two prominent peaks, and the I_D/I_G ratio values, which are consistent with earlier studies, indicate high-quality GQDs [27].

3.1.3 XRD Analysis of GQDs

X-ray diffraction (XRD) or electron diffraction (ED) is a useful technique for examining the structure of atomic materials and regularly obtain crystallographic structural information of materials with high accuracy. The XRD analysis provides structure, crystal orientation, mean particle size, crystal defects, and crystallinity [28]. Based on the efforts of Von Laue, W. H and W. L Bragg in 1913, now known as Bragg's law, defining the diffraction beam of a crystal described by Eq. (1) [29]:

$$\lambda = 2d_{hkl} \cdot \sin\theta \quad (1)$$

Where λ is wavelength X-ray and d_{hkl} is inter-planar/ interlayer spacing (nm), and is the diffraction angle. Figure 4 displays XRD pattern of GQDs.

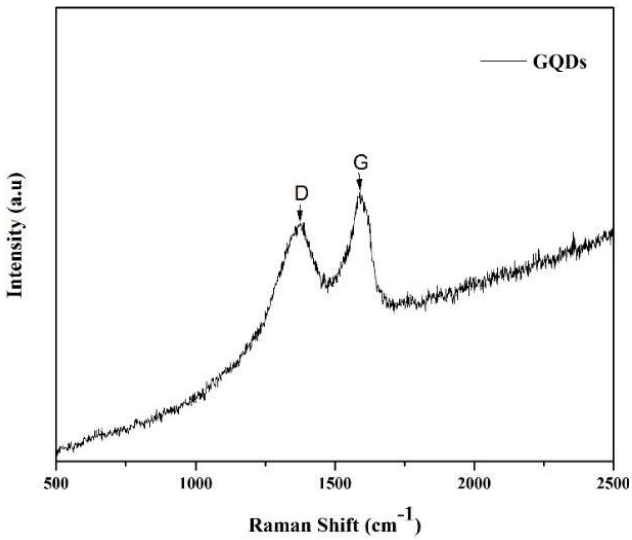

Figure 3. Raman Spectroscopy Analysis of GQDs.

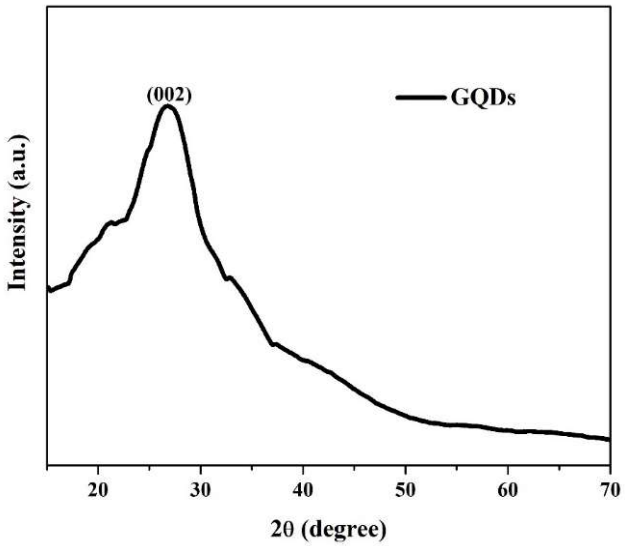

Figure 4. XRD Analysis of GQDs.

A weak broad, which can be described to the (002) as lattice spacing of graphene, shows a diffraction peak mid-pointed at $2\theta = 26.62^{o}$, relating to an inter-planar spacing at ca. 0.34 nm is wider than graphite [30, 31]. In the spectrum for GQDs, the other peak at 2 indicates the disordered stacking structure of graphene layers [17]. As sighted in another report, XRD analysis of GQDs with 2θ in the range 25^{o} - 30^{o} points to the structure of a graphene crystal in which GQDs were synthesized from commercially available graphene nano-powder [32].

3.1.4 Photoluminescence (PL) Spectroscopy Analysis of GQDs

The GQDs PL Spectrum usually has excitation around 350 nm, consistent with previous photoluminescence analyses [33]. Figure 5 shows GQDs PL Spectrum, the PL spectrum under a particular absorption band (350 nm) determined to the π-π* transition of graphitic sp^2 domains [30].

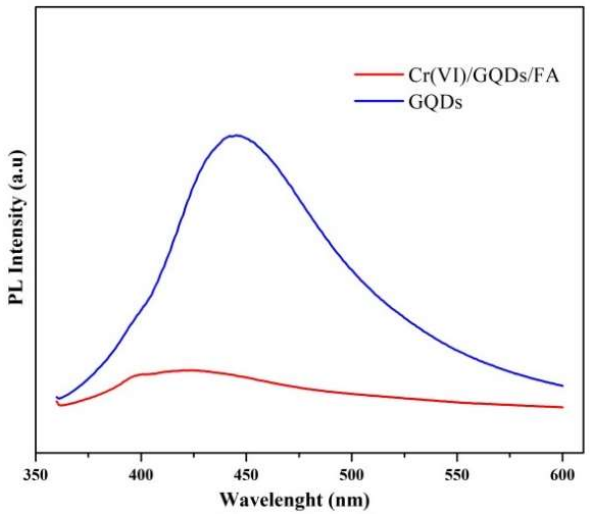

Figure 5. PL spectrum of GQDs and photocatalytic solution (Cr (VI)/GQDs/FA).

GQDs emits an intense PL spectrum at 450 nm when excited at 350 nm from these emission peaks than the Cr (VI)/GQDs/FA sample, where the PL is quenched completely. This identifies that GQDs have good PL properties that can be used as semiconductor materials, where the PL spectrum with the transition energy levels obtained shows its ability to absorb photons and excite electrons [34].

3.2. Reaction Conditions and Mechanisms of Photocatalytic Reduction

Figure 6 (a) shows the impact of light irradiation on the photocatalytic process of Cr (VI) degradation performance between the ratio degradation efficiency of Cr (VI) and the reaction time. Cr (VI) degradation efficiency percentages reached 12.7%, 18.3%, 85.4%, and 91.1% within the reaction time of 30 min for GQDs/FA; GQDs/Uv-vis; FA/Uv-vis; and GQDs/FA/Uv-vis system, respectively. From Figure 6 (a), the two parameters, Uv-vis and reduction agent (FA), significantly reduce Cr (VI). In GQDs/FA without Uv-vis, it displays that the reduction of Cr (VI) is negligible, as well as GQDs/Uv-vis without FA. Interestingly, FA/Uv-vis without GQDs could reduce Cr (VI) up to 85.5%, but the combination of GQDs/FA/Uv-vis increased the degradation by up to 90%. The extra Cr (VI) reduction ratio was obtained due to the role of GQDs as a photocatalyst with photoluminescence properties. In addition, GQDs can also speed up the photocatalytic process, where GQDs/FA/Uv-vis system drops significantly with the ratio of degradation efficiency of up to 62.26% at 24 minutes' interval time and 39.1% at 30 minutes' interval time if compared to FA/Uv-vis system. Thus, the participation of FA as a reduction agent and GQDs as a catalyst is relevant and reached good performance under Uv-vis light irradiation in the photocatalytic Cr (VI) reduction process [35].

As shown in Figure 6 (b), the reactions reached high performance with increasing the FA dose. The initial degradation percentages of Cr (VI) are low at 18.3% without the addition of FA. When the FA added about 1.0 mL and 2.0 mL, the Cr (VI) degradation percentages were obtained at 91.1% and 92.9%, respectively. Then at 3.0 mL FA, the increase in Cr (VI) reduction tends to stabilize. This phenomenon occurs because it has reached the optimum condition of the solution in generating hydrogen ions and carbon dioxide anion radicals ($CO_2^{\bullet-}$) in photocatalytic Cr (VI) degradation [10].

As seen in Figure 6 (c), without the addition of GQDs, reduction of Cr (VI) can be achieved at 85.4%. Then, by adding 1.0 mL GQDs, Cr (VI) reduction with an extra 6% can be increased. In the other addition, 2.0 mL GQDs, Cr (VI) reduction can be achieved up to 97.5% in 30 minutes. This increase is due to GQDs, which can be explained by kinetic energy under Uv-vis light irradiation, the formation of additional free electrons in the conduction

band, and carbon dioxide anion radicals ($CO_2^{\bullet-}$) can be all attributed to these results [36].

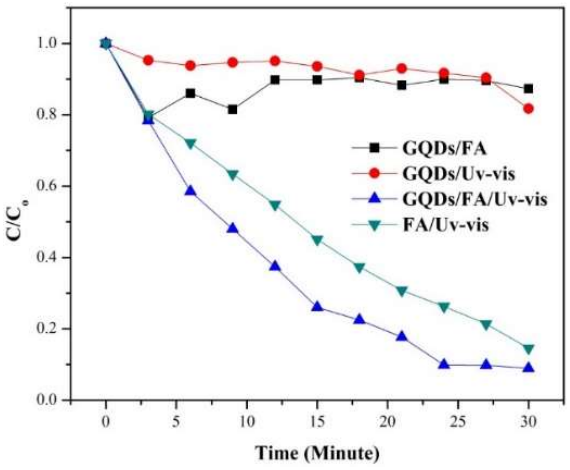

(a)

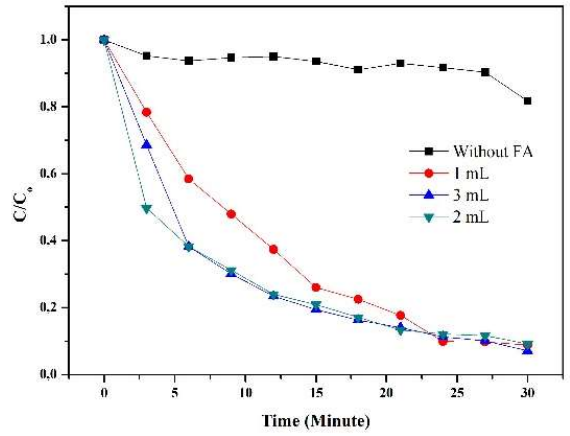

(b)

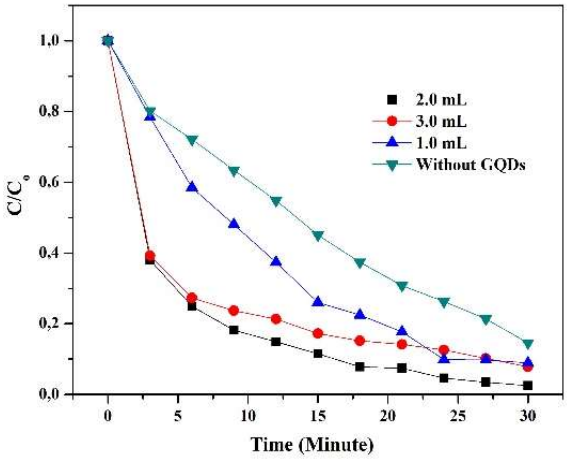

(c)

Figure 6. Photocatalytic reduction of Cr (VI) by GQDs. Effect of different light irradiation (a); different FA concentrations (b); different GQDs concentrations (c). All initial at 1 mL GQDs, 1 mL FA with the initial K2Cr2O7 of 40 mg/L, pH of 5.42.

Meanwhile, the consequence of initial Cr (VI) concentration on photocatalytic reduction is shown in Figure 7 (a). The result demonstrates an inverse correlation between Cr (VI) degradation and initial Cr (VI) concentration. Reduction of Cr (VI) is effective at low concentrations, where increasing the concentration will reduce the effectiveness of Cr (VI). It can be observed that with 40 and 20 mg/L of Cr (VI) is very effective using GQDs, where 20-45 mg/L of Cr (VI) is commonly found in the textile industry [37].

Furthermore, the interesting finding is found that the ability of GQDs is not only practical with low Cr (VI) concentration but also to time. To which 40 mg/L of Cr (VI) takes 30 minutes while 20 mg/L of Cr (VI) takes 15 minutes for the Cr (VI) reduction process. Because of the decomposition of FA, this condition produces abundant hydrogen as a reducing agent on the surface of the GQDs photo-catalyst; therefore, it only takes a short time to degrade Cr (VI) [4].

The pH of the solution is one of the most critical factors affecting the photocatalytic reduction as shown in Figure 7 (b); the acidic conditions are not favorable in the degradation of Cr (VI). Cr (VI) reduction with GQDs/FA/Uv-vis system at pH 3.0 and pH 4.0 showed a low degradation rate, meaning Cr (VI) reduction is more significant at pH conditions above 4.0. Where for pH 3.0; 4.0; and 5.42, the Cr (VI) degradation percentages were obtained at 45.18%; 80.4%; and 83.24%, respectively. It is slightly different from earlier research [38].

The degradation of Cr is significantly effective under acidic solution. Several researchers reported that the more decreasing pH, the higher positive charge (H^+) formed on the catalyst surface, resulting benefit in reduction Cr VI) to Cr (III). Meanwhile the significant Cr (VI) degradation using GQDs was observed at pH 5.42 (above pH 4.0), This indicates that GQDs was easily soluble below a neutral pH; this suggests that Cr (VI) reduction in the semiconductor catalyst is more effective at pH above 4.0 [39].

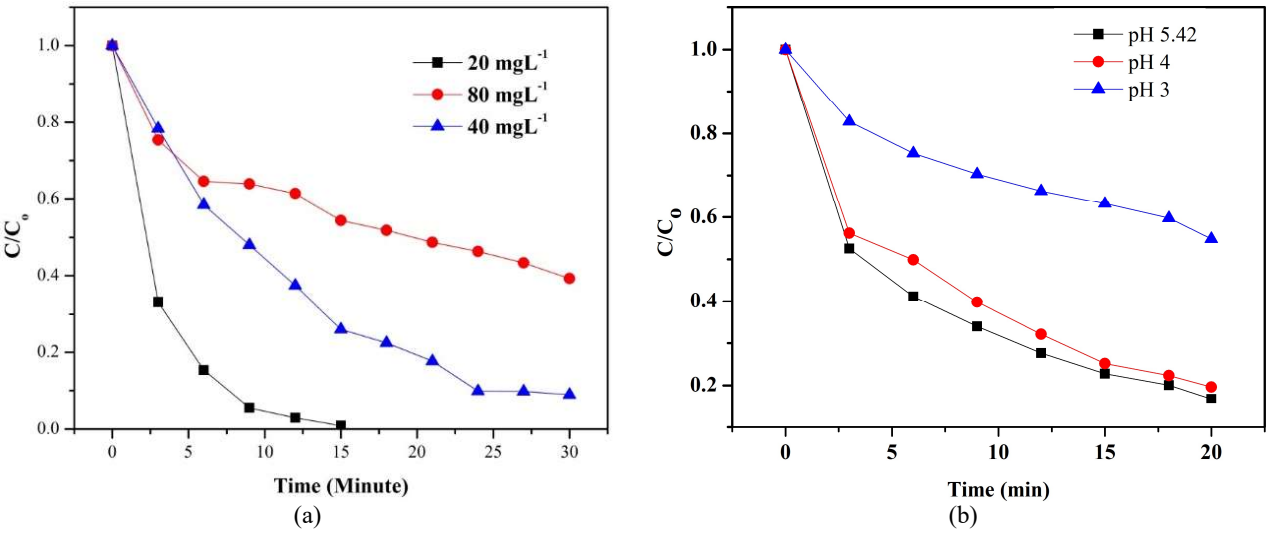

Figure 7. Photocatalytic reduction of Cr (VI) by GQDs. Effect of different Cr (VI) concentrations (a); different solution pH (b). All initial at 1 mL GQDs, 1 mL FA with the initial $K_2Cr_2O_7$ of 40 mg/L, pH of 5.42.

3.3. Proposed Mechanisms and kinetic rate of Photocatalytic Cr (VI) Reduction

Photocatalysis is a phenomenon using energy equal to or more than the bandgap energy (ΔEg) of the semiconductor catalyst, which is utilized to catalyze processes. In this research, by using GQDs excites hole (h^+) and electron (e^-) to the valence bands (VB) and the empty conduction bands (CB), respectively (Eq. 2,3) [9].

$$GQDs + hv \rightarrow GQDs–h^+ + GQDs– e^- \quad (2)$$

$$GQDs–h^+ + GQDs–e^- \rightarrow GQDs–h^+(VB) + GQDs–e^- (CB) \quad (3)$$

As semiconductor catalyst, GQDs has a band gap energy (ΔE_g) approximately at 2.71 eV [40].

The photocatalysis mechanism is based on the idea of semiconductor catalysis, in which electrons are stimulated by light of a suitable wavelength to move from VB to CB.

Furthermore, the light photo-generated electrons (e^-) react with oxygen to generate peroxy radicals ($O_2^{\bullet-}$) (Eq. 4). However, these photo-generated electrons cannot reduce Cr (VI) without FA. The presence of FA reacting with the photo-generated hole (h^+) in the photocatalytic reduction is the formation of a carbon dioxide anion radical ($CO_2^{\bullet-}$), which determines the main activity for the Cr (VI) degradation (Eq. 5) [10].

$$O_2 + e^- \rightarrow O_2^{\bullet-} \quad (4)$$

$$HCOO^- + h^+ \rightarrow CO_2^{\bullet-} + H^+ \quad (5)$$

Furthermore, the greatly reductive radicals ($CO_2^{\bullet-}$) were qualified to reduce the dichromate ions ($Cr_2O_7^{2-}$) through the reaction (Eq. 6). In the photocatalytic process of Cr (VI) reduction, N-N Dimethyl Aniline (N-N DA) was utilized as a radical scavenger to quench $CO_2^{\bullet-}$ radical as shown in Figure 8 (a) [10]. After applying N-N Dimethyl Aniline (N-N DA) into the GQDs/FA/Cr (VI) system, the degradation ratio progressively decreased, demonstrating that $CO_2^{\bullet-}$ radicals were the primary radicals generated during Cr (VI) degradation, with the majority of them quenched.

$$Cr_2O_7^{2-} + 14H^+ + 6CO_2^{\bullet-} \rightarrow 2Cr^{3+} + 7H_2O + 6CO_2 \quad (6)$$

The modified Langmuir-Hinshelwood kinetics model provides kinetic information using the pseudo-first-order model (Eq. 7) [41]:

$$\ln\frac{[Cr(VI)]}{[Cr(VI)]_o} = -k_{obs}t \quad (7)$$

Where [Cr (VI)] and [Cr (VI)]o are the final t time and initial time of Cr (VI) concentrations (mg/L), and kobs represent the pseudo-first-order rate constant (min^{-1}).

Figure 8 (b) plots ln [Cr (VI)/ Cr (VI)o] vs time to give the kinetic data at GQDs/FA/Uv-vis system. From the slope of ln [Cr(VI)/Cr(VI)o] vs time plots, the pseudo-first-order rate constant (k_{obs}) was calculated to be 0.10847 min^{-1}. Furthermore, the linear regression coefficient (R^2) was 0.985. This result was consistent with previous research, with R^2 values ranging from 0.979 to 0.997 [42].

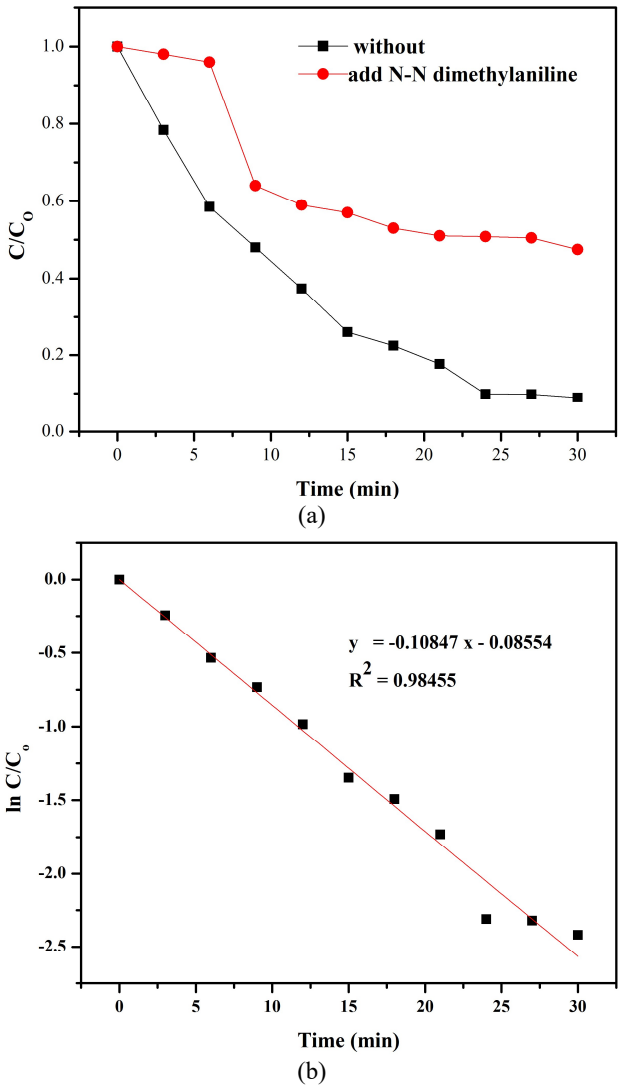

Figure 8. Effect of quenching $CO_2^{\bullet-}$ radical (a); ln [Cr (VI)/Cr (VI)$_o$] *vs.* t-plots (b). Conditions GQDs/FA/Uv-vis of Cr (VI) photocatalytic reduction: 1 mL GQDs, 1 mL FA, and 40 mg/L $K_2Cr_2O_7$, 1 mL of N-N DA, pH 5.42.

Table 1 lists the pseudo-first-order rate constant (k_{obs}) from other systems.

Table 1. The Pseudo-First-Order Rate Constant and the Linear Regression Coefficient from various systems.

Systems	R^2	k_{obs} (min^{-1})
GQDs/FA	0.66078	0.0139
GQDs/Uv-vis	0.00036	-0.1072
FA/Uv-vis	0.98247	0.0468
GQDs/FA/Uv-vis	0.98455	0.1085

The modified Langmuir-Hinshelwood kinetic model can be adapted from plots of the initial concentration rate (r) and initial Cr (VI) concentration in a heterogeneous photocatalytic process(Eq. 8,9) [43-45]:

$$r = k_c \frac{K_{Cr(VI)}[Cr(VI)]_o}{1 + K_{Cr(VI)}[Cr(VI)]} = k_{obs}[Cr(VI)] \quad (8)$$

$$\frac{1}{k_{obs}} = \frac{1}{k_c K_{Cr(VI)}} + \frac{[Cr(VI)]_o}{k_c} \quad (9)$$

Where $K_{Cr(VI)}$ (L/mg) represents the Langmuir-Hinshelwood adsorption equilibrium constant and kc ($mg^{-1}Lmin^{-1}$) represents the surface reaction kinetic rate constant.

By plotting 1/*k*obs vs Cr $(VI)_O$ give the slope and intercept of the linear regression (Table 2), are $K_{Cr(VI)}$ at 0.0537 L mg^{-1} and k_c 1.6556 mg/L min, respectively. As comparison, photocatalytic reduction of Cr (VI) using Fe_2O_3/clay reached constant $K_{Cr(VI)}$ (0.052 L/mg) and k_c (0.893 mg/L min) [44], and Cr (VI) reduction using ZnO reached the rate constant k_c at 0.8245 mg/Lmin [46]. Thus, Cr (VI) reduction using GQDs/FA is higher than Fe_2O_3/clay and ZnO.

Table 2. k_{obs} kinetic parameters at various Cr (VI) initial concentration.

$[Cr(VI)]_O$ (mg/L)	R^2	k_{abs} (min^{-1})	$1/k_{abs}$ (min)
80	0.92462	0.0261	38.31418
40	0.98455	0.1085	9.21914
20	0.99461	0.3025	3.30579

4. Conclusion

In conclusion, this study successfully demonstrated the effectiveness of Graphene Quantum Dots (GQDs) as a photocatalyst for the degradation of Cr (VI) using Uv-vis light irradiation and formic acid (FA) as a reductive agent. The characterization of GQDs revealed critical insights into their properties. XPS analysis showed a high percentage of carbon elements, indicating the substantial contribution of GQDs to photocatalytic activity. Raman spectroscopy provided information on the crystalline size and defect rates of GQDs. XRD analysis confirmed the presence of a graphene crystal structure in GQDs. PL spectroscopy demonstrated the emission of a solid luminescent spectrum by GQDs.

The photocatalytic reduction of Cr (VI) achieved its highest performance using the GQDs/FA/Uv-vis system. The solution's optimal pH was 5.42, as GQDs exhibited better solubility below neutral pH. The photocatalytic process exhibited a remarkable kinetic reaction, with a degradation efficiency of 91.1%. The kinetic parameters, including the rate constant (k) and the coefficient of determination (R^2), followed the pseudo-first-order model with values of 0.1085 min^{-1} and 0.985, respectively. The photocatalytic reduction mechanism involved the generation of $CO_2^{\bullet-}$ as the primary active radical responsible for reducing Cr (VI) to the more environmentally friendly Cr (III). These findings highlight the potential of using GQDs and FA under Uv-vis light for efficiently degrading Cr (VI) to Cr (III). However, further research is warranted to explore the applicability of GQDs with other reduction agents in the remediation of other pollutants. The insights gained from this study contribute to the prospects of utilizing GQDs in environmental remediation applications.

Acknowledgments

We acknowledge Zhejiang Normal University and the Chinese Scholarship Council (CSC) for financially supporting this research and The Ministry of Education and Culture of Indonesia (Kemendikbud) and LPDP for gradually supporting for complete writing through the 2011 World Class Professional (WCP) Program.

Competing Interest Statement

The authors declare no known competing financial interests or personal relationships that could have influenced the work reported in this paper.

Data and Materials Accessibility

Supplementary materials and data used in this research are accessible upon request. For access, please contact the corresponding author.

References

[1] Z. Liu, G. Wang, and X. Zhao, "Removal of Cr (VI) from aqueous solution using ultrafine coal fly ash," *Journal of Wuhan University of Technology-Mater. Sci. Ed.,* vol. 25, pp. 323-327, 2010.

[2] R. N. Bharagava and S. Mishra, "Hexavalent chromium reduction potential of Cellulosimicrobium sp. isolated from common effluent treatment plant of tannery industries," *Ecotoxicology and Environmental Safety,* vol. 147, pp. 102-109, 2018.

[3] M. Celebi, M. Yurderi, A. Bulut, M. Kaya, and M. Zahmakiran, "Palladium nanoparticles supported on amine-functionalized SiO2 for the catalytic hexavalent chromium reduction," *Applied Catalysis B: Environmental,* vol. 180, pp. 53-64, 2016.

[4] Y. Huang, H. Ma, S. Wang, M. Shen, R. Guo, X. Cao*, et al.*, "Efficient catalytic reduction of hexavalent chromium using palladium nanoparticle-immobilized electrospun polymer nanofibers," *ACS applied materials & interfaces,* vol. 4, pp. 3054-3061, 2012.

[5] J. J. Rueda-Marquez, I. Levchuk, P. F. Ibañez, and M. Sillanpää, "A critical review on application of photocatalysis for toxicity reduction of real wastewaters," *Journal of Cleaner Production,* vol. 258, p. 120694, 2020.

[6] J. Dodson, A. Hunt, H. Parker, Y. Yang, and J. Clark, "Elemental sustainability: Towards the total recovery of scarce metals," *Chemical Engineering and Processing: Process Intensification,* vol. 51, pp. 69-78, 2012.

[7] W. Chen, G. Lv, W. Hu, D. Li, S. Chen, and Z. Dai, "Synthesis and applications of graphene quantum dots: a review," *Nanotechnology Reviews,* vol. 7, pp. 157-185, 2018.

[8] Y. Dong, J. Shao, C. Chen, H. Li, R. Wang, Y. Chi*, et al.*, "Blue luminescent graphene quantum dots and graphene

oxide prepared by tuning the carbonization degree of citric acid," *Carbon,* vol. 50, pp. 4738-4743, 2012.

[9] E. Karamian and S. Sharifnia, "On the general mechanism of photocatalytic reduction of CO2," *Journal of CO2 Utilization,* vol. 16, pp. 194-203, 2016.

[10] W. Song, P. Ge, Q. Ke, Y. Sun, F. Chen, H. Wang*, et al.*, "Insight into the mechanisms for hexavalent chromium reduction and sulfisoxazole degradation catalyzed by graphitic carbon nitride: the Yin and Yang in the photo-assisted processes," *Chemosphere,* vol. 221, pp. 166-174, 2019.

[11] J. B. Islam, M. Furukawa, I. Tateishi, H. Katsumata, and S. Kaneco, "Photocatalytic reduction of hexavalent chromium with nanosized TiO2 in presence of formic acid," *ChemEngineering,* vol. 3, p. 33, 2019.

[12] S. Dai, X. Wu, J. Zhang, Y. Fu, and W. Li, "Coenzyme A-regulated Pd nanocatalysts for formic acid-mediated reduction of hexavalent chromium," *Chemical Engineering Journal,* vol. 351, pp. 959-966, 2018.

[13] A. Ibarbia, H. J. Grande, and V. Ruiz, "On the factors behind the photocatalytic activity of graphene quantum dots for organic dye degradation," *Particle & Particle Systems Characterization,* vol. 37, p. 2000061, 2020.

[14] A. Nagaraj, M. A. Munusamy, A. A. Al-Arfaj, and M. Rajan, "Functional ionic liquid-capped graphene quantum dots for chromium removal from chromium contaminated water," *Journal of Chemical & Engineering Data,* vol. 64, pp. 651-667, 2018.

[15] W.-M. Yang, F. Liu, Y.-T. Jin, Z.-M. Dong, and G.-C. Zhao, "Efficient reduction of Cr (VI) with carbon quantum dots," *ACS omega,* vol. 7, pp. 23555-23565, 2022.

[16] G. F. Moreira, E. R. Peçanha, M. B. Monte, L. S. Leal Filho, and F. Stavale, "XPS study on the mechanism of starch-hematite surface chemical complexation," *Minerals Engineering,* vol. 110, pp. 96-103, 2017.

[17] S. Wang, X. Chu, X. Xiang, and Y. Cao, "Highly selective antenna effect of graphene quantum dots (GQDs): A new fluorescent sensitizer for rare earth element terbium in aqueous media," *Talanta,* vol. 209, p. 120504, 2020.

[18] T. Van Tam, S. G. Kang, K. F. Babu, E.-S. Oh, S. G. Lee, and W. M. Choi, "Synthesis of B-doped graphene quantum dots as a metal-free electrocatalyst for the oxygen reduction reaction," *Journal of Materials Chemistry A,* vol. 5, pp. 10537-10543, 2017.

[19] S. Sarkar, D. Gandla, Y. Venkatesh, P. R. Bangal, S. Ghosh, Y. Yang*, et al.*, "Graphene quantum dots from graphite by liquid exfoliation showing excitation-independent emission, fluorescence upconversion and delayed fluorescence," *Physical Chemistry Chemical Physics,* vol. 18, pp. 21278-21287, 2016.

[20] S. Zhu, J. Zhang, X. Liu, B. Li, X. Wang, S. Tang*, et al.*, "Graphene quantum dots with controllable surface oxidation, tunable fluorescence and up-conversion emission," *Rsc Advances,* vol. 2, pp. 2717-2720, 2012.

[21] T. Ogi, H. Iwasaki, K. Aishima, F. Iskandar, W.-N. Wang, K. Takimiya*, et al.*, "Transient nature of graphene quantum dot formation via a hydrothermal reaction," *Rsc Advances,* vol. 4, pp. 55709-55715, 2014.

[22] C. Zhu, S. Yang, G. Wang, R. Mo, P. He, J. Sun*, et al.*, "Negative induction effect of graphite N on graphene quantum dots: tunable band gap photoluminescence," *Journal of Materials Chemistry C,* vol. 3, pp. 8810-8816, 2015.

[23] E. Petrova, S. Tinchev, and P. Nikolova, "Interference effects on the ID/IG ratio of the Raman spectra of diamond-like carbon thin films," *arXiv preprint arXiv:1112.0897,* 2011.

[24] A. C. Ferrari and D. M. Basko, "Raman spectroscopy as a versatile tool for studying the properties of graphene," *Nature nanotechnology,* vol. 8, pp. 235-246, 2013.

[25] S. Kim, D. Hee Shin, C. Oh Kim, S. Seok Kang, S. Sin Joo, S.-H. Choi*, et al.*, "Size-dependence of Raman scattering from graphene quantum dots: interplay between shape and thickness," *Applied Physics Letters,* vol. 102, p. 053108, 2013.

[26] J.-S. Yang, D. A. Martinez, and W.-H. Chiang, "Synthesis, characterization and applications of graphene quantum dots," in *Recent Trends in Nanomaterials*, ed: Springer, 2017, pp. 65-120.

[27] P. Luo, X. Guan, Y. Yu, X. Li, and F. Yan, "Hydrothermal synthesis of graphene quantum dots supported on three-dimensional graphene for supercapacitors," *Nanomaterials,* vol. 9, p. 201, 2019.

[28] R. Kohli, "Methods for monitoring and measuring cleanliness of surfaces," in *Developments in Surface Contamination and Cleaning*, ed: Elsevier, 2012, pp. 107-178.

[29] A. A. Bunaciu, E. G. UdriŞTioiu, and H. Y. Aboul-Enein, "X-ray diffraction: instrumentation and applications," *Critical reviews in analytical chemistry,* vol. 45, pp. 289-299, 2015.

[30] M. Xie, Y. Su, X. Lu, Y. Zhang, Z. Yang, and Y. Zhang, "Blue and green photoluminescence graphene quantum dots synthesized from carbon fibers," *Materials Letters,* vol. 93, pp. 161-164, 2013.

[31] R. Zhang and Z. Ding, "Recent advances in graphene quantum dots as bioimaging probes," *Journal of Analysis and Testing,* vol. 2, pp. 45-60, 2018.

[32] M. J. Deka, A. Dutta, and D. Chowdhury, "Tuning the wettability and photoluminescence of graphene quantum dots via covalent modification," *New Journal of Chemistry,* vol. 42, pp. 355-362, 2018.

[33] Z. Gan, H. Xu, and Y. Hao, "Mechanism for excitation-dependent photoluminescence from graphene quantum dots and other graphene oxide derivates: consensus, debates and challenges," *Nanoscale,* vol. 8, pp. 7794-7807, 2016.

[34] T. H. Gfroerer, "Photoluminescence in analysis of surfaces and interfaces," *Encyclopedia of analytical chemistry,* vol. 67, p. 3810, 2000.

[35] S. Zhu, Y. Song, J. Wang, H. Wan, Y. Zhang, Y. Ning*, et al.*, "Photoluminescence mechanism in graphene quantum dots: Quantum confinement effect and surface/edge state," *Nano Today,* vol. 13, pp. 10-14, 2017.

[36] M. Naimi-Joubani, M. Shirzad-Siboni, J.-K. Yang, M. Gholami, and M. Farzadkia, "Photocatalytic reduction of hexavalent chromium with illuminated ZnO/TiO2 composite," *Journal of industrial and engineering chemistry,* vol. 22, pp. 317-323, 2015.

[37] K. Cirik, N. Dursun, E. Sahinkaya, and Ö. Çinar, "Effect of electron donor source on the treatment of Cr (VI)-containing textile wastewater using sulfate-reducing fluidized bed reactors (FBRs)," *Bioresource technology,* vol. 133, pp. 414-420, 2013.

[38] Z. Zhao, H. An, J. Lin, M. Feng, V. Murugadoss, T. Ding*, et al.*, "Progress on the photocatalytic reduction removal of chromium contamination," *The Chemical Record,* vol. 19, pp. 873-882, 2019.

[39] M. Samarghandi, J. Yang, S. Lee, O. Giahi, and M. Shirzad-Siboni, "Effect of different type of organic compounds on the photocatalytic reduction of Cr (VI) in presence of ZnO nanoparticles," *Desalination and water treatment,* vol. 52, pp. 1531-1538, 2014.

[40] S. S. Mousavi, A. Kazempour, B. Efafi, M. H. M. Ara, and B. Sajad, "Effects of graphene quantum dots interlayer on performance of ZnO-based photodetectors," *Applied Surface Science,* vol. 493, pp. 1187-1194, 2019.

[41] M. Roushani, M. Mavaei, and H. R. Rajabi, "Graphene quantum dots as novel and green nano-materials for the visible-light-driven photocatalytic degradation of cationic dye," *Journal of Molecular Catalysis A: Chemical,* vol. 409, pp. 102-109, 2015.

[42] M. A. Omole, I. O. K'Owino, and O. A. Sadik, "Palladium nanoparticles for catalytic reduction of Cr (VI) using formic acid," *Applied Catalysis B: Environmental,* vol. 76, pp. 158-167, 2007.

[43] M.-R. Samarghandi, J.-K. Yang, O. Giahi, and M. Shirzad-Siboni, "Photocatalytic reduction of hexavalent chromium with illuminated amorphous FeOOH," *Environmental technology,* vol. 36, pp. 1132-1140, 2015.

[44] H. Mekatel, S. Amokrane, B. Bellal, M. Trari, and D. Nibou, "Photocatalytic reduction of Cr (VI) on nanosized Fe2O3 supported on natural Algerian clay: characteristics, kinetic and thermodynamic study," *Chemical engineering journal,* vol. 200, pp. 611-618, 2012.

[45] M. A. Behnajady, N. Mansoriieh, N. Modirshahla, and M. Shokri, "Influence of operational parameters and kinetics analysis on the photocatalytic reduction of Cr (VI) by immobilized ZnO," *Environmental technology,* vol. 33, pp. 265-271, 2012.

[46] S. Chakrabarti, B. Chaudhuri, S. Bhattacharjee, A. K. Ray, and B. K. Dutta, "Photo-reduction of hexavalent chromium in aqueous solution in the presence of zinc oxide as semiconductor catalyst," *Chemical Engineering Journal,* vol. 153, pp. 86-93, 2009.